Disentangling Multidimensional Nonequilibrium Dynamics of Adsorbates: CO Desorption from Cu(100)

Ken-ichi Inoue,* Kazuya Watanabe,† Toshiki Sugimoto, and Yoshiyasu Matsumoto
Department of Chemistry, Graduate School of Science, Kyoto University, Kyoto 606-8502, Japan

Tomokazu Yasuike‡
Department of Liberal Arts, The Open University of Japan, Chiba 261-8586, Japan
(Received 6 April 2016; published 26 October 2016)

Hot carriers at metal surfaces can drive nonthermal reactions of adsorbates. Characterizing nonequilibrium statistics among various degrees of freedom in an ultrafast time scale is crucial to understand and develop hot carrier-driven chemistry. Here we demonstrate multidimensional vibrational dynamics of carbon monoxide (CO) on Cu(100) along hot-carrier induced desorption studied by using time-resolved vibrational sum-frequency generation with phase-sensitive detection. Instantaneous frequency and amplitude of the CO internal stretching mode are tracked with a subpicosecond time resolution that is shorter than the vibrational dephasing time. These experimental results in combination with numerical analysis based on Langevin simulations enable us to extract nonequilibrium distributions of external vibrational modes of desorbing molecules. Superstatistical distributions are generated with mode-dependent frictional couplings in a few hundred femtoseconds after hot-electron excitation, and energy flow from hot electrons and intermode anharmonic coupling play crucial roles in the subsequent evolution of the non-Boltzman distributions.

DOI: 10.1103/PhysRevLett.117.186101

Hot-carrier induced surface reaction of adsorbates on metal is triggered nonthermally by high-temperature electrons, which are generated by irradiation of metal with an intense femtosecond laser pulse [1–13] or by excitation of the localized surface plasmon of metallic nanoparticles [14–17]. Ultrafast energy transfer from electrons in metal to adsorbate nuclear degrees of freedom (DOF) via nonadiabatic coupling [18–25] is of fundamental importance because it induces novel surface reactions [14,26,27].

Despite extensive studies at flat metal surfaces over decades [26], our understanding of the ultrafast energy flow during hot-carrier induced reactions is still in its infancy. Earlier two-pulse correlation studies [1,3–5,8–11,28] have specified the time scale of reactions and provided rich information on energy partitioning in desorption by product state analysis but were incapable of probing vibrational dynamics. Ultrafast time-resolved vibrational spectroscopy, particularly probing the internal stretching mode (S mode) of diatomic adsorbates [12,29,30], has been used to track excitation of external vibrational modes: frustrated translation (FT), frustrated rotation (FR), and external stretch (ES) modes. While the frequency shift of the S mode is dominated by coupling with the FT mode under moderate excitation [31–35], intense fs pulse excitation leads to larger S-mode frequency shifts due to hot-carrier driven FR mode excitation; thus, the FR mode was considered to trigger lateral hopping [12] and/or desorption of adsorbates [36,37]. Because the time resolution of the time-resolved vibrational sum-frequency generation (TR-VSFG) studies is inherently limited by an S-mode dephasing time ($\sim$1 ps), it has not been possible to clarify the dynamics in the sub-ps time scale, including the intermode coupling effects between FR and FT as well as ES modes that are crucial in the hot-carrier induced reactions [38–40]. Furthermore, lack of a theoretical estimate of coupling strength between the S mode and external modes prevents us from estimating the excitation degrees of external modes quantitatively from the observed S-mode frequency shift.

In contrast to a prevailing belief that mode-dependent nonadiabatic couplings in hot-carrier induced reactions lead to different temperatures among the vibrational modes of adsorbate [41], recent theoretical studies on hot-carrier induced H_2 desorption have shown that all desorption product properties are described with a single effective temperature due to rapid vibrational energy redistribution [23]. While this seems to be specific to light adsorbates, it arouses a renewed interest in ultrafast statistics during hot-carrier induced reactions: how large are their deviations from Boltzmann distributions and their mode dependence in the ultrafast time scale?

In this work, we have focused on hot-carrier induced desorption of carbon monoxide (CO) on Cu(100) to clarify the interplay of the external modes as well as their nonequilibrium statistics in the sub-ps time scale. In several earlier studies on the laser-induced desorption dynamics on CO/Ru(0001) [29,42], the dominating mechanism has been found to be phonon-induced desorption. Here, Cu substrate is chosen because the small electron-phonon

coupling in bulk Cu allows us to minimize the effect of substrate phonons [32]. By using TR-VSFG with phase-sensitive detection [43,44], we have measured the instantaneous frequency (ω_{CO}) shift and amplitude decay of the S mode during the hot-carrier induced desorption with a time resolution shorter than the S-mode dephasing time. We have further carried out Langevin simulation [25] on a reliable multidimensional potential energy surface (PES) [45]; comparison of calculated ω_{CO} shifts with those determined experimentally enables us to extract evolution of the external modes in an unprecedented manner.

Experiments were conducted with a TR-VSFG setup combined with an ultrahigh vacuum chamber [Fig. 1(c)] [46]. Prior to each measurement, CO gas was dosed at 100 K on a Cu(100) single crystal, forming a saturated monolayer confirmed by a low energy electron diffraction [55,56]. Because pump (400 nm, 150 fs) -induced desorption decreases the coverage during the measurement, CO was dosed continuously to keep a constant coverage [46]. The phase-sensitive measurement [57] was attained by mixing the SFG signal from the sample and that from a "local oscillator," a nonlinear optical crystal, by varying their relative phase with BaF_2 wedged plates, both real and imaginary parts of the vibrational response function can be obtained [46].

Figure 1(d) shows pump induced changes in the real and imaginary parts of S-mode responses as a function of pump-IR delay time, Δt [Fig. 1(b)]. The excitation of external modes by hot electrons manifests itself as transient

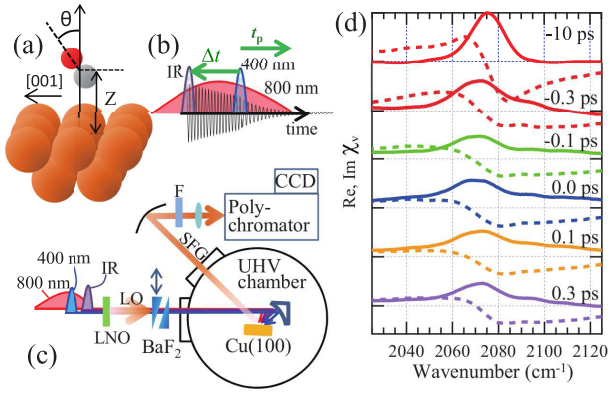

FIG. 1. (a) Coordinates used for simulating desorption dynamics of CO on Cu(100): the distance of the molecular center of mass from the surface Cu atom (Z) and the molecular tilting angle (θ, only a tilting to [001] direction is considered). (b) Schematic of a pulse sequence, indicating a pump-IR delay time, Δt, and a time elapsed following the pump pulse, t_p. The oscillatory curve schematically represents S-mode polarization. Note that the figure shows the case of $\Delta t < 0$. (c) Experimental setup for the time-resolved SFG with a phase-sensitive detection [46]. Filter (F), local oscillator (LO), and $LiNbO_3$ crystal (LNO). (d) The real (broken lines) and the imaginary part (solid lines) of the time-resolved vibrational response spectra of CO on Cu(100) with 400 nm pump. Delay times, Δt, are indicated in the figure.

broadenings and peak shifts of the band for $\Delta t \geq -0.3$ ps. The time evolution of S-mode vibrational polarization perturbed by the external modes [Fig. 2(a)] can be obtained by using the inverse Fourier transform of the distorted spectra [44,46]. Hereafter, we focus on the results obtained at $\Delta t = -0.3$ ps. (see Sec. II of the Supplemental Material [46]).

Figure 2(b) shows instantaneous frequency shifts of the S mode, $\Delta\omega_{CO}$, obtained by time-resolved Fourier analysis of the vibrational polarization [44]. At a moderate pump fluence, the peak frequency shows monotonic red-shifts as a function of elapsed time after the pump pulse, t_p [Fig. 1(b)], while at the highest fluence, the peak shifts to higher frequency after reaching the maximum red shift (at $t_p = 0.15$ ps). The transient polarization also contains amplitude information. Figure 2(b) (bottom) shows the pump induced relative change of the amplitude of the vibrational polarization $R(t_p)$. The S-mode amplitude decay is accelerated with increasing pump fluence.

To extract the time evolution of the external motions of CO from the peak frequency shifts and amplitudes obtained experimentally, we have carried out numerical simulations based on the Langevin equation derived with the influence functional method [25], which has been employed in previous works [22,58,59]. We employ here a restricted dimensional model with minimal degrees of freedom, Z and θ [see Fig. 1(a)] (see Sec. IV of the Supplemental Material for the justification of the model [46]) and a recently presented analytical expression of the multidimensional PES of CO/Cu(100), SAP-PES [45]. Denoting the coordinate Z or θ as X and its conjugate momentum as p_X,

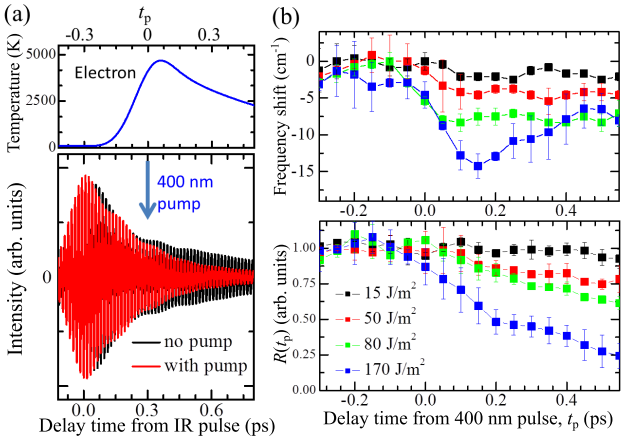

FIG. 2. (a) (Top) Time dependence of T_e calculated from the two temperature model for pump fluence of 170 J/m^2. (Bottom) Retrieved C-O vibrational coherence (polarization) for without (black) and with (red) pump pulse irradiated at $\Delta t = -0.3$ ps. (b) Pump fluence dependence of (top) $\Delta\omega_{CO}$ estimated from the time-shifted Fourier transform of the S-mode polarization, and (bottom) the ratio of the amplitude of the vibrational coherence with and without pump pulse irradiation as a function of t_p, $R(t_p)$.

the working equations determining the time evolutions of X and p_X are given by

$$dX(t) = p_X(t)/\mathcal{M}_{\mathrm{CO}}, \tag{1}$$

$$dp_X(t) = -\{\partial V(Z(t),\theta(t))/\partial X + \eta_X(t)p_X(t)\}dt + \sqrt{2\mathcal{M}_{\mathrm{CO}}\eta_X(t)k_B T_e(t)}dW(t), \tag{2}$$

where $\mathcal{M}_{\mathrm{CO}}$ is mass of CO (moment of inertia of CO) for the Z coordinate (θ coordinate). $V(Z(t),\theta(t))$ is the 2D potential function derived from SAP-PES [shown in Fig. 3(e)(left)], k_B is the Boltzmann constant, $W(t)$ is a one-dimensional Wiener process, and $\eta_Z(t)$ and $\eta_\theta(t)$ are the friction coefficients for the Z and θ coordinates, respectively. Time-varying electron temperature $T_e(t)$ was determined separately by numerically solving the coupled thermal diffusion equations with the experimental laser absorbed fluence and pulse width [32,60]. The time dependence of η was incorporated through $T_e(t)$ dependence of the friction coefficients [25,46]. For η at 0 K, we used the values estimated by Krishna and Tully [61] ($1/3.8$ and $1/13.7$ ps^{-1} for FR and ES mode, respectively) with a scaling factor of 2 (see Sec. IV of the Supplemental Material [46]), and ignored their coordinate dependence because signals come from molecules mainly confined within the adsorption well in contrast to some previous studies which focused on desorption yields [22,58,59].

We also estimated the Z and θ dependence of ω_{CO} by the normal mode analysis of the SAP-PES [Fig. 3(e)(right)]. The obtained $\omega_{\mathrm{CO}}(Z,\theta)$ map shows clear features: ω_{CO} continuously redshifts with increasing in θ at around $\Delta Z = 0$ and blueshifts for $\Delta Z < 0$ and $\Delta Z \gtrsim 0.5a_0$ at around $\theta = 0$, where $\Delta Z = Z - Z_{\mathrm{eq}}$ is a displacement from the equilibrium point Z_{eq}. (For justification of the instantaneous normal mode analysis see Sec. V in the Supplemental Material [46]).

We run 3000 trajectories for each parameter after equilibrating the system for 1 ps at 100 K and estimated instantaneous frequencies by averaging $\omega_{\mathrm{CO}}(Z,\theta)$ with the computed statistical distribution $P(Z,\theta)$. In addition, the decay of the S-mode polarization $R(t_p)$ was simulated by taking account of the following factors: population damping enhancement by hot carriers, dephasing by the frequency modulation concomitant with the external modes excitation, and signal intensity decrease by molecular tilting (FR mode excitation) (see sec. VI of the Supplemental Material [46] for details). Actual trajectories can be seen in movies in the Supplemental Material [46], and the contour plots of their density snapshots are depicted in Fig. 3(f).

Figures 3(a) and 3(b) show comparisons of the experimental $\Delta\omega_{\mathrm{CO}}$ and $R(t_p)$ with moving average over 0.2 ps of the calculated values by the Langevin simulation, respectively. The simulations account for the experimental $\Delta\omega_{\mathrm{CO}}$ quantitatively both at low (50 J/m^2) and high (170 J/m^2) fluences. The amplitude decays [Fig. 3(b)] are qualitatively simulated (solid curves) except for some discrepancies. To analyze contributions of several factors in the simulated $R(t_p)$ at the high fluence, the simulations with only the dephasing effect (green-dotted curve) and with both the damping and dephasing effects (excluding the orientation factor, green-dot-dashed curve) are also shown in Fig. 3(b). While the damping effects dominates for $t_p < 0.2$ ps, the dephasing contribution grows at $t_p > 0.2$ ps. The discrepancies between the experiments and the simulations are possibly due to neglecting the modulations in the S-mode dynamic dipole and Raman

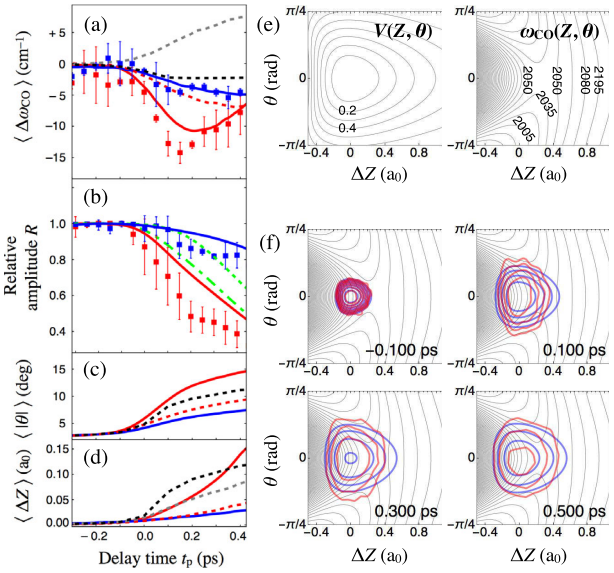

FIG. 3. (a),(b) Comparison between experimental and simulation results of t_p dependence of (a) the instantaneous frequency shift of CO stretching mode $\langle\Delta\omega_{\mathrm{CO}}\rangle$ and (b) the relative vibrational amplitude $R(t_p)$. (c),(d) The simulation results of (c) tilt angle $\langle|\theta|\rangle$ and (d) the ES mode displacement $\langle\Delta Z\rangle$ (in unit of Bohr radius, a_0). Full simulation results are depicted by solid curves while experimental ones are plotted by filled squares. The pump fluences are 170 (red) and 50 J/m^2 (blue). Dotted curves in (a),(c),(d) are simulation results for 170 J/m^2 with restricted conditions: (red) with temperature independent ηs (ηs at 0 K), (gray) with the 1D simulation results with only ES mode and (black) with 2D Boltzmann distributions depicted with blue contours in (f) (see text). Green curves in (b) are simulations of $R(t_p)$ for 170 J/m^2 including only the dephasing effect (dotted curve) and including both the damping and dephasing effects (dot-dashed curve). (e) Contour maps in the (Z,θ) coordinates of adsorption potential (left, in units of eV) and C-O stretching frequency ω_{CO} (right, in units of cm^{-1}). The point $(\Delta Z,\theta) = (0,0)$ corresponds to the minimum of adsorption potential (on-top site, upright configuration). (f) (Red lines) Logarithmic contour plots of snap shots of $P(Z,\theta)$ with a pump fluence of 170 J/m^2 at t_p indicated in figures. (Blue lines) Logarithmic contour plots of the Boltzmann distributions with T_{2D} in Fig. 4(b) (see text). The backgrounds are the contour maps of ω_{CO}, same as (e) (right).

tensor as a function of the (Z, θ) coordinates. In addition, recently predicted coupling between the S and ES modes due to the off-diagonal elements of the friction tensor [62] can contribute to the discrepancies.

Varying some parameters in the simulation reveals the necessary ingredients of the observed features. The red dotted curves in Figs. 3(a), 3(c), and 3(d) show simulations at the highest fluence in which the T_e dependence of ηs has been omitted. Clearly, neglecting the T_e dependence (with ηs at 0 K) results in much moderate excitation of both the coordinates, showing the importance of the T_e dependence of η; this has been pointed out both experimentally [11] and theoretically [25] but is confirmed here in the time-resolved fashion for the first time. We further examined the robustness of the simulation results on the assumed density of states of the unoccupied state (see Sec. IV of the Supplemental Material [46]).

The transient "shift-back" feature in $\Delta\omega_{\mathrm{CO}}$ at the highest fluence in Fig. 3(a) is explained as follows; first, $P(Z, \theta)$ is elongated along the θ axis because of $\eta_\theta > \eta_Z$, which causes the red shift of ω_{CO} [Fig. 3(f), 0.1 ps]. The excitation in θ is clearly demonstrated in Fig. 3(c) where $\langle|\theta|\rangle$ extracted from the simulations are plotted. At $t_p \geqq 0.3$ ps, $P(Z, \theta)$ spreads along the Z axis covering the region with high ω_{CO} values, leading to the relative blueshift. Figure 3(d) shows the time evolution of $\langle\Delta Z\rangle$ estimated from the simulations, indicating a delay in exciting the motion along the Z coordinate compared to the θ coordinate. Analysis of the trajectories revealed that not only direct excitation along the Z coordinate by hot electrons, but also indirect heating by an energy flow from the FR mode largely contributes through the intermode coupling by the potential $V(Z, \theta)$. This is evidenced by comparison with a 1D Langevin simulation including only the ES mode (Z coordinate), as indicated by the gray-dotted curve in Fig. 3(d), which shows less pronounced excitation of $\langle\Delta Z\rangle$ than that in the 2D simulation with the intermode coupling.

Nonequilibrium distributions among the CO-substrate vibrational modes causing the aforementioned ω_{CO} shifts are estimated by analyzing the kinetic energy distributions in the simulation at the highest fluence. Figures 4(a) and 4(b) show the number of DOF n^X_{DOF} and effective temperatures T_X, respectively, for $\mathrm{X} = Z$, θ, and two dimensions including both the FR and ES modes. They are derived from the gamma-distribution fitting of the kinetic energies at given t_p (see Sec. VIII of the Supplemental Material [46]). If the system was in dynamic equilibrium described with time-dependent Boltzmann distributions, the following conditions should be satisfied: $n^{\mathrm{2D}}_{\mathrm{DOF}} = 2$, $n^Z_{\mathrm{DOF}} = n^\theta_{\mathrm{DOF}} = 1$, and $T_{\mathrm{2D}} = T_Z = T_\theta$. Any deviations from these conditions are sensitive indicators of the nonequilibrium feature of the system.

If energy distributions in multiple DOFs are described with Boltzmann distributions of different temperatures, this type of nonequilibrium is called "superstatistical"

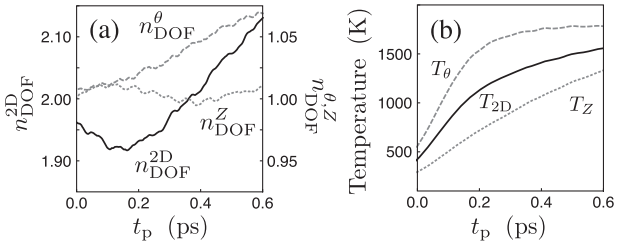

FIG. 4. (a) Time evolution of the number of DOF for gamma distribution functions of the computed kinetic energies. (b) Time evolution of the effective temperatures estimated from expectation values of kinetic energies [46]. In both figures, the solid, dashed, and dotted curves represent 2D(FR and ES), FR, and ES modes, respectively.

[63]. In general, the system consisting of weakly coupled subsystems tends to show superstatistical features. Figure 4 shows that at $t_p < 0.1$ ps, where the contour plot is elongated along the θ coordinate [Fig. 3(f)], the system is in a superstatistical distribution because $n_{\mathrm{DOF}} \sim 1$ for both θ and Z while $n^{\mathrm{2D}}_{\mathrm{DOF}}$ deviates from two, $T_Z < T_\theta$ due to the large difference in η. Therefore, the intermode coupling between FR and ES is not effective enough at $t_p < 0.1$ ps. At $t_p > 0.1$ ps, as adsorbates are excited more extensively along θ, the intermode coupling due to the potential anharmonicity becomes operative to accelerate excitation along the Z coordinate. The simulation with mode-independent coefficients (see Sec. IX of the Supplemental Material [46]) shows $T_Z = T_\theta$, whereas each mode deviates from the equilibrium distribution; thus, the emergence of the superstatistical situation is attributed to the mode dependence of the friction coefficients. Here only the diagonal elements of the friction tensors have been considered in the current simulation. Recently, the off-diagonal friction coefficient between the S and ES mode has been predicted to be significant [62]. A rapid energy flow from the S to ES mode due to the off-diagonal term may reduce the superstatistical feature.

At $t_p > 0.4$ ps, the system evolves in a more general nonequilibrium state; although T_Z and T_θ merge gradually due to the intermode coupling [Fig. 4(b)], $n^{\mathrm{2D}}_{\mathrm{DOF}}$ further deviates from two [Fig. 4(a)]. This is because hot electrons maintains a heat flow into the FR mode, leading to growing deviations of n^θ_{DOF} from one [Fig. 4(a)]. In contrast, the ES mode keeps nearly Boltzmann distributions, $n^Z_{\mathrm{DOF}} \sim 1$: the existence of such an effectively isolated canonical subsystem is not trivial under the highly nonequilibrium conditions. This is probably because of the small friction coefficient of the ES mode: the small agitation keeps the local quasiequilibrium, which is generally observed in slowly relaxing systems effectively characterized by small friction coefficients [64]. Figure 3(f) shows the contour plots of 2D Boltzmann distributions with temperatures the same as T_{2D} depicted in Fig. 4(b). $\langle\Delta\omega_{\mathrm{CO}}\rangle(t_p)$ calculated by using the 2D Boltzmann distributions gives only

negligible frequency shifts indicated by the black-dotted curve in Fig. 3(a). This demonstrates that the aforementioned deviations of $n_{\mathrm{DOF}}^{\mathrm{2D}}$ from two are the origin of the peculiar t_p-dependent shift in $\Delta\omega_{\mathrm{CO}}$ observed.

In summary, we have extracted the hot-electron induced nonequilibrium dynamics of CO on Cu(100) by comparing vibrational dynamics of the S-mode with the Langevin type simulation in which ES and FR DOFs are considered. The nonequilibrium dynamics are caused by the mode- and the T_e-dependent frictional coefficients and the intermode couplings on the multidimensional PES. These features are expected to play important roles in other hot-carrier induced surface reactions and deserve considerations in analysis of experiments including recently emerging novel techniques [42].

This work was supported by JSPS KAKENHI Grants No. 2662006 and No. 15K05394. We acknowledge Yuji Otsuki for his assistance in the early stage of the calculation.

*Present address: RIKEN.
†kw@kuchem.kyoto-u.ac.jp
‡yasuike@ouj.ac.jp
Also at ESICB, Kyoto University.

[1] J. A. Prybyla, T. F. Heinz, J. A. Misewich, M. M. T. Loy, and J. H. Glownia, Phys. Rev. Lett. **64**, 1537 (1990).
[2] J. A. Prybyla, H. W. K. Tom, and G. D. Aumiller, Phys. Rev. Lett. **68**, 503 (1992).
[3] F. Budde, T. F. Heinz, M. M. T. Loy, J. A. Misewich, F. de Rougemont, and H. Zacharias, Phys. Rev. Lett. **66**, 3024 (1991).
[4] F. J. Kao, D. G. Busch, D. Cohen, D. GomesdaCosta, and W. Ho, Phys. Rev. Lett. **71**, 2094 (1993).
[5] F. J. Kao, D. G. Busch, D. GomesdaCosta, and W. Ho, Phys. Rev. Lett. **70**, 4098 (1993).
[6] J. A. Misewich, T. F. Heinz, and D. M. Newns, Phys. Rev. Lett. **68**, 3737 (1992).
[7] D. G. Busch, S. Gao, R. A. Pelak, M. F. Booth, and W. Ho, Phys. Rev. Lett. **75**, 673 (1995).
[8] L. M. Struck, L. J. Richter, S. A. Buntin, R. R. Cavanagh, and J. C. Stephenson, Phys. Rev. Lett. **77**, 4576 (1996).
[9] M. Bonn, S. Funk, C. Hess, D. N. Denzler, C. Stempfl, M. Scheffler, M. Wolf, and G. Ertl, Science **285**, 1042 (1999).
[10] D. N. Denzler, C. Frischkorn, C. Hess, M. Wolf, and G. Ertl, Phys. Rev. Lett. **91**, 226102 (2003).
[11] K. Stépán, J. Güdde, and U. Höfer, Phys. Rev. Lett. **94**, 236103 (2005).
[12] E. H. G. Backus, A. Eichler, A. W. Kleyn, and M. Bonn, Science **310**, 1790 (2005).
[13] M. Lawrenz, K. Stépán, J. Güdde, and U. Höfer, Phys. Rev. B **80**, 075429 (2009).
[14] M. L. Brongersma, N. J. Halas, and P. Nordlander, Nat. Nanotechnol. **10**, 25 (2015).
[15] S. Mukherjee, F. Libisch, N. Large, O. Neumann, L. V. Brown, J. Cheng, J. B. Lassiter, E. A. Carter, P. Nordlander, and N. J. Halas, Nano Lett. **13**, 240 (2013).
[16] P. Christopher, H. Xin, and S. Linic, Nat. Chem. **3**, 467 (2011).
[17] Y. Kang, S. Najmaei, Z. Liu, Y. Bao, Y. Wang, X. Zhu, N. J. Halas, P. Nordlander, P. M. Ajayan, J. Lou, and Z. Fang, Adv. Mater. **26**, 6467 (2014).
[18] J. W. Gadzuk, in *Handbook of Surface Science Vol. 3 Dynamics*, edited by E. Hasselbrink and B. I. Lundqvist (Elsevier, Amsterdam, 2008), Chap. 1, p. 2.
[19] A. M. Wodtke, D. Matsiev, and D. J. Auerbach, Prog. Surf. Sci. **83**, 167 (2008).
[20] B. I. Lundqvist and A. Hellman, in *Handbook of Surface Science Vol. 3 Dynamics*, edited by E. Hasselbrink and B. I. Lundqvist (Elsevier, Amsterdam, 2008), Chap. 10, p. 429.
[21] J. C. Tully, Annu. Rev. Phys. Chem. **51**, 153 (2000).
[22] A. C. Luntz, M. Persson, S. Wagner, C. Frischkorn, and M. Wolf, J. Chem. Phys. **124**, 244702 (2006).
[23] G. Füchsel, J. C. Tremblay, T. Klamroth, P. Saalfrank, and C. Frischkorn, Phys. Rev. Lett. **109**, 098303 (2012).
[24] J. C. Tully, M. Gomes, and M. Head-Gordon, J. Vac. Sci. Technol. A **11**, 1914 (1993).
[25] M. Brandbyge, P. Hedegard, T. F. Heinz, J. A. Misewich, and D. M. Newns, Phys. Rev. B **52**, 6042 (1995).
[26] C. Frischkorn and M. Wolf, Chem. Rev. **106**, 4207 (2006).
[27] P. Saalfrank, Chem. Rev. **106**, 4116 (2006).
[28] F. Budde, T. F. Heinz, A. Kalamarides, M. M. T. Loy, and J. A. Misewich, Surf. Sci. **283**, 143 (1993).
[29] M. Bonn, C. Hess, S. Funk, J. H. Miners, B. N. J. Persson, M. Wolf, and G. Ertl, Phys. Rev. Lett. **84**, 4653 (2000).
[30] I. M. Lane, D. A. King, Z.-P. Liu, and H. Arnolds, Phys. Rev. Lett. **97**, 186105 (2006).
[31] B. N. J. Persson and R. Ryberg, Phys. Rev. Lett. **54**, 2119 (1985).
[32] T. A. Germer, J. C. Stephenson, E. J. Heilweil, and R. R. Cavanagh, J. Chem. Phys. **101**, 1704 (1994).
[33] T. A. Germer, J. C. Stephenson, E. J. Heilweil, and R. R. Cavanagh, Phys. Rev. Lett. **71**, 3327 (1993).
[34] T. A. Germer, J. C. Stephenson, E. J. Heilweil, and R. R. Cavanagh, J. Chem. Phys. **98**, 9986 (1993).
[35] M. Nagao, K. Watanabe, and Y. Matsumoto, J. Phys. Chem. C **113**, 11712 (2009).
[36] F. Fournier, W. Zheng, S. Carrez, H. Dubost, and B. Bourguignon, Phys. Rev. Lett. **92**, 216102 (2004).
[37] C. Springer and M. Head-Gordon, Chem. Phys. **205**, 73 (1996).
[38] B. N. J. Persson and H. Ueba, Phys. Rev. B **76**, 125401 (2007).
[39] H. Ueba, M. Hayashi, M. Paulsson, and B. N. J. Persson, Phys. Rev. B **78**, 113408 (2008).
[40] H. Ueba and B. N. J. Persson, Phys. Rev. B **77**, 035413 (2008).
[41] J. A. Misewich, T. F. Heinz, P. Weigand, and A. Kalamarides, in *Laser Spectroscopy and Photochemistry on Metal Surfaces*, edited by H.-L. Dai and W. Ho (World Scientific, Singapore, 1995), Chap. 19, p. 764.
[42] M. Dell'Angela *et al.*, Science **339**, 1302 (2013).
[43] K. Watanabe, K.-i. Inoue, I. F. Nakai, and Y. Matsumoto, Phys. Rev. B **81**, 241408 (2010).
[44] K.-i. Inoue, K. Watanabe, and Y. Matsumoto, J. Chem. Phys. **137**, 024704 (2012).

[45] R. Marquardt, F. Cuvelier, R. A. Olsen, E. J. Baerends, J. C. Tremblay, and P. Saalfrank, J. Chem. Phys. **132**, 074108 (2010).
[46] See Supplemental Material at http://link.aps.org/supplemental/10.1103/PhysRevLett.117.186101 for details of the experimental setup, data analysis, and the Langevin simulations, which contains Refs. [47–54].
[47] R. Superfine, J. Y. Huang, and Y. R. Shen, Opt. Lett. **15**, 1276 (1990).
[48] K. C. Chou, S. Westerberg, Y. R. Shen, P. N. Ross, and G. A. Somorjai, Phys. Rev. B **69**, 153413 (2004).
[49] T. F. Heinz, in *Nonlinear Surface Electromagnetic Phenomena*, edited by H. E. Ponath and G. I. Stegeman (Elsevier, 1991), Chap. 5, p. 353.
[50] P. Galletto, H. Unterhalt, and G. Rupprechter, Chem. Phys. Lett. **367**, 785 (2003).
[51] C. J. Hirschmugl, Y. J. Chabal, F. M. Hoffmann, and G. P. Williams, J. Vac. Sci. Technol. A **12**, 2229 (1994).
[52] J. Rogozik, V. Dose, K. C. Prince, A. M. Bradshaw, P. S. Bagus, K. Hermann, and Ph. Avouris, Phys. Rev. B **32**, 4296 (1985).
[53] B. N. J. Persson and R. Ryberg, Phys. Rev. B **24**, 6954 (1981).
[54] M. Morin, N. J. Levinos, and A. L. Harris, J. Chem. Phys. **96**, 3950 (1992).
[55] A. P. Graham, F. Hofmann, J. P. Toennies, G. P. Williams, C. J. Hirschmugl, and J. Ellis, J. Chem. Phys. **108**, 7825 (1998).
[56] E. Borguet and H. Dai, J. Chem. Phys. **101**, 9080 (1994).
[57] N. Ji, V. Ostroverkhov, C. Y. Chen, and Y. R. Shen, J. Am. Chem. Soc. **129**, 10056 (2007).
[58] T. Olsen and J. Schiotz, J. Chem. Phys. **133**, 034115 (2010).
[59] G. Füchsel, T. Klamroth, S. Monturet, and P. Saalfrank, Phys. Chem. Chem. Phys. **13**, 8659 (2011).
[60] S. I. Anisimov, B. L. Kapeliovich, and T. L. Perel'man, Sov. Phys. JETP **39**, 375 (1974).
[61] V. Krishna and J. C. Tully, J. Chem. Phys. **125**, 054706 (2006).
[62] M. Askerka, R. J. Maurer, V. S. Batista, and J. C. Tully, Phys. Rev. Lett. **116**, 217601 (2016).
[63] C. Beck and E. Cohen, Physica (Amsterdam) **322A**, 267 (2003).
[64] D. Regera, J. M. Rubi, and J. M. G. Vilar, J. Phys. Chem. B **109**, 21502 (2005).